Transportation Research Interdisciplinary Perspectives 25 (2024) 101108

Contents lists available at ScienceDirect

Transportation Research Interdisciplinary Perspectives

journal homepage: www.elsevier.com/locate/trip

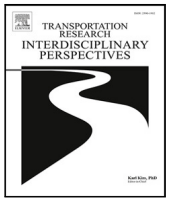

On the practical utility of a continuum traffic flow model on curvy highways in adverse weather conditions

Waheed Imran [a,*], Zawar H. Khan [b], Daud Khan [c], Usman Ghani [d], Tahseen Bashir [a]

[a] Department of Civil, Architectural and Environmental Engineering, University of Naples, Via Claudio 21, Naples, 80125, Italy
[b] College of Computer Science and Engineering, University of Ha'il, Ha'il, 55476, Saudi Arabia
[c] Department of Transport Systems, Traffic Engineering and Logistics, Faculty of Transport and Aviation Engineering, Silesian University of Technology, Krasinskiego 8 Street, Katowice, 40019, Poland
[d] Department of Engineering, Ed.8, University of Palermo, Viale Delle Scienze, Palermo, 90128, Italy

ARTICLE INFO

Keywords:
Adverse weather conditions
Curvy highways
Macroscopic continuum model
Non-Homogeneous-Stimulus-Response model
Traffic dynamics
Traffic forecasting

ABSTRACT

The macroscopic continuum traffic flow models are being investigated to predict and ameliorate traffic more efficiently. These models are beneficial implementation tools to comprehend and complement the shortfalls in traffic evolution. Despite the significant enhancements in devising the traffic dynamics, the practical utilization of these macroscopic models is not being fully explored. In this study, the Non-Homogeneous Stimulus-Response Model (NHSRM) (Imran et al., 2023) is investigated for its application in forecasting traffic flow on a curvy highway during various weather conditions. The weather impact, in the specific, dry, light rainfall, moderate rainfall, and heavy rainfall on the travel time, velocity, and density spatiotemporal evolution on a curvy highway is analyzed. The flow during different weather conditions is investigated over two curved roads with 120 m, and 500 m radii. As evident from the results, significant velocity breakdowns during heavy rainfall impact the upstream traffic which contributes to congestion development. The average velocity of traffic depletes significantly, and the congestion formation upstream is significant. While the travel time of particular highway segments elevates sharply during heavy rainfall. A comprehensive understanding of the insights, and the criticality associated with the parameters of the model, in particular, on the choice of the maximum velocity of the highway has been presented for NHSRM.

1. Introduction

Macroscopic continuum flow models play a pivotal role in forecasting and understanding complex traffic flow behavior on highways (Imran et al., 2020). These models provide a detailed representation of complex traffic behavior and have long been applauded for their potential applications in infrastructure planning, traffic management, and Intelligent Transportation Systems (ITS). The macroscopic continuum traffic models supply significant insights into the overall traffic dynamics, allowing urban planners and policymakers to make informed decisions for improving the efficiency and safety of highways. Moreover, macroscopic models are significantly revised to improve their characterization accuracy and effectiveness during employment.

With the advent of modern data collection techniques and evolving computing capabilities, various traffic influencing factors are incorporated within the macroscopic traffic flow models. These factors include traffic driver behavior, road network characteristics, and weather conditions. By integrating these diverse characteristics, contemporary macroscopic models have become more robust and capable of providing realistic representations of real-world traffic scenarios (Jiang et al., 2002).

Weather conditions, in particular, have a significant impact on traffic flow and travel time on highways. Adverse weather conditions, including fog, snow, and heavy rainfall. These can lead to reduced visibility and decreased friction on road surfaces. These are detrimental to traffic flow, resulting in hazardous traffic incidents, and consequently, impacting traffic flow operations. Drivers reduce their speeds during adverse weather conditions to be more cautious and precise in vehicle control as conditions are more predictable, and has a tendency of large variations in traffic velocity. This increases the following distances between vehicles which decreases traffic flow (Brackstone and McDonald, 2007; Qu et al., 2014). Moreover, adverse weather often necessitates the activation of various control measures, including traffic control with variable speed limits, lane closures, or even road closures, which further disrupts the traffic.

Nevertheless, the significant progress made in expanding macroscopic traffic flow models to encompass various aspects of road traffic,

* Corresponding author.
E-mail address: waheed.imran@unina.it (W. Imran).

https://doi.org/10.1016/j.trip.2024.101108
Received 13 August 2023; Received in revised form 16 March 2024; Accepted 5 May 2024
Available online 13 May 2024

as well as their practical applicability in hazardous weather conditions, has not been fully exercised. Further, the conceptual breakthroughs and incorporation of multiple factors open up exciting avenues for utilizing these models in real-world settings. However, realizing their full practical potential requires extensive investigation and robust methodologies in the context of various weather conditions. This investigation is crucial to identify the strengths and limitations of the models and to assess their feasibility for addressing practical traffic management challenges.

In view of the aforementioned rationale, the key contributions of this paper are summarized as

1. The macroscopic continuum Non-Homogeneous Stimulus-Response Model (NHSRM) (Imran et al., 2023) is studied in this paper to assess the traffic evolution over different road geometry in different weather conditions. And, in particular, upstream velocity and density evolution is investigated.
2. Additionally, the weather conditions impact on travel time is highlighted which offers significant insights into real-world traffic management. It is demonstrated that weather data integration with NHSRM can be employed in weather-adaptive traffic management strategies for traffic amelioration.
3. This study presents a comprehensive methodology for NHSRM utilization in adverse weather conditions.

The rest of this paper is organized as follows. A detailed review of the existing related literature is presented in Section 2. In Section 3, the methodology including the continuum model, fundamentals of traffic, and the settings for simulations are presented. The results of this study are given in Section 4, while a brief discussion of the results is detailed in Section 5. Finally, some conclusions are given in Section 6.

2. Literature review

Typically, macroscopic traffic models examine the aggregate density, velocity, and flow (Kessels et al., 2019). While in microscopic models, physical and psychological driver behavior/individual vehicle behavior are considered (Nagel et al., 2003; Henein and White, 2010). The characteristics of both, macroscopic and microscopic models are coupled in mesoscopic models (Cantarella et al., 2014) and probability distributions are mostly harnessed (Kessels et al., 2019; Hoogendoorn and Bovy, 2001). The macroscopic models are commonly exercised due to their modest computational complexity (Khan et al., 2019).

The foundation of macroscopic models was laid by the Lighthill, Whitham, and Richards (LWR) model (Lighthill and Whitham, 1955; Richards, 1956). The LWR model is expressed as

$$\rho_t + \rho(V(\rho))_x = 0, \tag{1}$$

where ρ and $V(\rho)$ are density, and the relationship in equilibrium traffic conditions between velocity and density, respectively. This relation is referred to as the equilibrium velocity relationship in what follows and is given by Eq. (6). In Eq. (1), the subscript t is the temporal derivative while x is the spatial derivative. Traffic is assumed a continuum in the LWR model, and only models trivial variations in traffic occurring instantly, that is, ideal traffic conditions on a highway. Thus, this model cannot precisely describe and characterize sufficient variations in traffic (Liu et al., 1998a) such as stop and go waves (Daganzo, 1995; Khan and Gulliver, 2018; Maerivoet and De Moor, 2005; Khan et al., 2022b). The LWR model was significantly improved by adding an acceleration term (Khan et al., 2019). Based on a car following theory, a higher-order traffic flow model was proposed by Payne (Zhang, 1998; Payne, 1971). This model considers changes in traffic flow based on a uniform driver response (anticipation). To characterize the driver's reaction to preceding stimuli an anticipation term was proposed while a relaxation term to characterize variations in velocity (Maerivoet and De Moor, 2005). Whitham proposed a similar model, and so the new model is known as the Payne Whitham (PW) model (Khan and Gulliver, 2019; Khan et al., 2018), given by

$$\begin{cases} \rho_t + \rho(V(\rho))_x = 0, \\ (\rho v)_t + \left(\frac{(\rho v)^2}{\rho} + C_0^2\rho\right)_x = \rho\left(\frac{V(\rho)-v}{\tau}\right), \end{cases} \tag{2}$$

where the velocity constant (C_0^2) represents the backward perturbation propagation speed and $\frac{V(\rho)-v}{\tau}$ is the relaxation term. Alignment of traffic over the relaxation time τ is characterized by the relaxation term. However, the PW model incorporates a uniform behavior for all vehicles (Whitham, 2011) which is unrealistic in practicality as vehicle behavior varies according to various traffic conditions (Imran et al., 2023). Consequently, the PW model can result in unsatisfactory outcomes (Zhang, 1998; Imran et al., 2023).

Lately, the PW model has been extended in various directions. As the objective of our study pertains to real-world utility rather than focusing on the development and enhancements of the models, we have directed our attention towards pertinent literature encompassing continuum macroscopic models, which can be found within the referenced papers such as Aw and Rascle (2000), Ko et al. (2015), Zhai and Wu (2022), Ngoduy (2013), Helbing et al. (2001), Liu et al. (1998b), Song and Karni (2019), Jiang and Wu (2004), Tang et al. (2011), Khan et al. (2022a), Zhai and Wu (2021) and Qingtao et al. (2018). All of these studies hold immense practical significance and can be employed for various practical applications in traffic analysis and control. However, in this study, we employ one of the finest macroscopic models proposed lately, the NHSRM (Imran et al., 2023), and is given by Eq. (3) to demonstrate its practical utility.

Evidently, traffic demand, safety, operation, and flow are significantly reduced (Maze et al., 2006) by rainfall, fog, snow, and wind. During adverse weather conditions, averaged data from sensors is harnessed to predict free flow speed and capacity. The HCM (2010) (Trans. Research Board, 2010) reports a reduction in capacity and free flow during adverse weather on highways. The FHWA (2006) has reported pragmatic studies on the impact of adverse weather on highways (Hranac et al., 2006). A mesoscopic network simulation (Hou et al., 2013) suggested that weather factors can be introduced in the calibration of the traffic flow model. The cold weather impact on highway traffic is studied by Shahdah and Fu (2010) based on simulations on a Canadian highway. The rainfall intensity impact on traffic speed, flow, and density is modeled (Lam et al., 2013) on hourly rainfall data in Hong Kong. These studies considered complex methodologies for traffic parameters estimations in different weather conditions. With evolving ITS, certain aspects of the HCM (Trans. Research Board, 2010) and American Association of State Highway and Transportation Officials (AASHTO) green book (AASHTO, 2011) can be coupled with the macroscopic models for more robust and accurate traffic flow, travel time, and velocity breakdowns predictions.

Another important aspect of a highway is the geometry such as sharp curves. Lamm et al. (1990) investigated the impacts on freeway capacity considering the geometry of curves during rainfall of rural highways. It has been reported that there is a significant relationship between operating speed and degree of curvature. But, in this study, it is also reported that wet pavement does not affect vehicle operating speed if visibility is not affected appreciably by heavy rainfall which is contrary to the fact that even light rainfall can reduce the friction between the tires and pavement, consequently, affecting the operating speed (Maze et al., 2006; Ibrahim and Hall, 1994). This fact has been further highlighted by Brilon and Ponzlet (1996), wet roadway conditions resulted in drops in velocity and capacity.

Kyte et al. (2001) studied the impacts of adverse weather on the capacity of a highway, and they have compared their results with the HCM (Trans. Research Board, 2010). It has been shown that a 50% reduction in speed resulted during light rainfall or light snow, conversely, heavy snow caused a lower reduction of 20% in speed compared to the

values suggested in Trans. Research Board (2010). Liang et al. (1998) conducted a similar study to Kyte et al. (2001) employing a shorter segment of the same test sites, while reporting a 5.03 m/s reduction in the average operating speed during snowfall. A predictor, Road Surface Condition (RSC) as a binary variable (1 if snow-covered, 0 otherwise) is incorporated in the regression analysis and a reduction of 1.50 m/s in the average speed is reported when the road surface was covered with snow. However, this binary representation of RSC does not capture the full variation of RSC that could commonly be observed in the real-world environment, moreover, there are more accurate methodologies with in-depth details about the road surf conditions such as the Pavement Condition Index (PCI). Furthermore, both of these two studies ignore the intensity of rainfall and were based on rural highways where traffic flows rarely reach capacity.

Ibrahim and Hall (1994) performed investigations, harnessing a Dummy Variable Multiple Regression Analysis Scheme (DVMRAS) to demonstrate the variations in traffic variables in various weather conditions (snow and rainfall). Their study reported that light snow and rainfall showed 3%, and up to 5% decrease in speeds, while heavy rainfall and snow caused 14% to 15% and 30% to 40% reductions in speed, respectively. However, the findings of their study are limited in generality as they were based on data obtained over six clear, two rainfall, and two snowy days.

In all, there are various vital limitations (as reported previously) of past efforts in quantifying the impacts of adverse weather on highway operations. The existing studies and methodologies are limited in practicality and are either too complex for real-time traffic management. Additionally, past studies do not investigate the impacts of weather conditions on jam formation and dissipation with a curved section, and avoid the increase in travel time due to the intensity of rainfall. While the velocity breakdowns are also not quantified on upstream traffic which is significant for traffic management. Further, the methodologies are complex and are based on odd data collection techniques, while with the evolution of the robust macroscopic models, certain aspects can be investigated more efficiently coupling with the Trans. Research Board (2010), AASHTO (2011) methodology which is rarely considered in recent studies. While the Trans. Research Board (2010), AASHTO (2011) have provided a set of adjustment factors for taking into consideration the winter weather effects, fewer studies have been conducted to show the validity of these results. But, these sets are never exercised in the framework of the macroscopic traffic flow model which can effectively describe different dynamics, vital for traffic flow planning and management such as jam formation, increase in the total travel time, and velocity breakdowns. Thus, in this study, the evolution of traffic flow on a 10,000 m highway is investigated. The geometry of the highway is composed of a sharp curve of radius 120 m and 500 m. The NHSRM is coupled with the highway traffic based on the guidelines provided in AASHTO (2011). Comprehensive evolution of density and velocity and variations in travel time are explored. In addition, an integrated methodology is proposed which can be efficiently employed in weather-adaptive control applications.

3. System

In this Section, the NHSRM and AASHTO (2011) coupled system is elaborated. The flow chart in Fig. 1 represents the detailed methodology of this study. Two distinct components are incorporated in the methodology forming an integrated system of the continuum model and the design parameter. At the outset, it entails the setup of the continuum model, next, the second facet incorporates the selection of design parameter based on the weather conditions on a curved highway, and their integration with the model, thereby resulting in an integrated system.

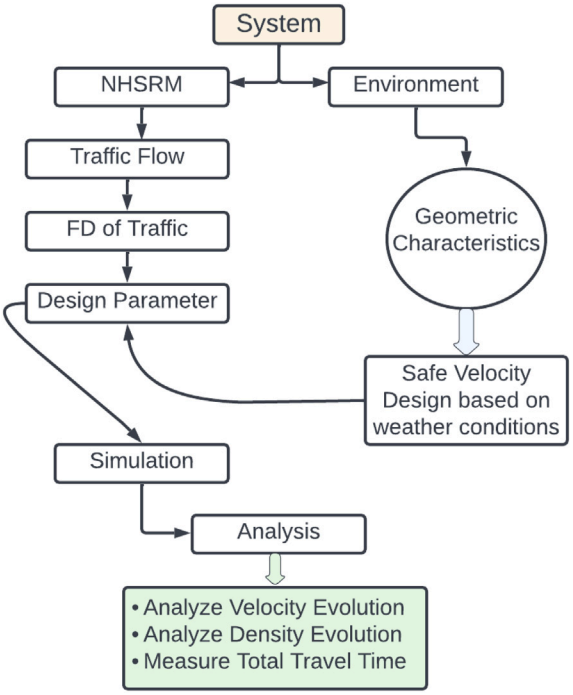

Fig. 1. The NHRSM and AASHTO (2011) coupled system.

3.1. The continuum model

The NHSRM (Imran et al., 2023) is a recent extension of the PW model which incorporates road stimulus and driver response to characterize traffic more realistically. NHSRM is

$$\begin{cases} \rho_t + \rho(V(\rho))_x = 0, \\ (\rho v)_t + \left(\frac{(\rho v)^2}{\rho} + f\varsigma\rho\right)_x = \rho\left(\frac{V(\rho)-v}{\tau}\right), \end{cases} \tag{3}$$

where

$$f = \left(\frac{|V(\rho) - v|}{v \times (\tau_r + \tau_b) + \frac{v^2}{2a_m}}\right), \tag{4}$$

is the driver response while

$$\varsigma = \frac{b_a}{b_m}, \tag{5}$$

is the stimulus. τ_r is the reaction time to a preceding change in traffic and τ_b is the harmonization time to adjust to this change. a_m is the maximum deceleration while b_a and b_m characterizes lateral distances. The ratio of which is a stimulus for a driver reaction. The Papageorgiou equilibrium velocity distribution (Papageorgiou et al., 1989) for $V(\rho)$ is used in this study, and is given by

$$V(\rho) = v_f \cdot \exp\left[\frac{-1}{c}\left(\frac{\rho}{\rho_{cr}}\right)^c\right], \tag{6}$$

where v_f is the free flow velocity, c is shape factor while ρ_{cr} is the critical density of the road section. This equilibrium distribution is exercised for its practical plausibility in any traffic condition. v_f is crucial for precise predictions in any given traffic conditions. It can vary according to different traffic conditions. That is, in dry weather conditions, v_f is higher, while it is smaller during heavy rainfall. The free flow speed, which is the maximum achievable, is also affected by road designed geometry of a highway. The selection of the maximum speed is significant to avoid road accidents and improve the traffic flow. Thus selection of v_f plays a vital role in traffic characterization in different road geometries in various conditions.

3.2. Highway characteristics

Road geometry is critical for traffic operations and has unique challenges to road safety which results from the centrifugal forces generated actively during sharp and moderate curves. This can drift the vehicle from the pavement for a speed higher than the safe speed. Optimal velocity over the curves is vital to ensure smooth, efficient, and accident-free traffic operations. Moreover, sharp curves during various weather conditions are detrimental to traffic flow operations. Safe velocity, v_s, over these curves can be computed (AASHTO, 2011) as

$$v_s = \sqrt{\mu R g}, \tag{7}$$

which is the allowed maximum achievable for vehicles traveling over road geometric curves, therefore, $v_s = v_f$. In Eq. (7), R is the radius of curvature. μ is the coefficient of friction between the pavement and tires of a vehicle, whereas g is the gravitational acceleration.

The significance of Eq. (7) lies in its practical application to determine safe velocity on curved road sections. Traffic engineers utilize this formula to assess appropriate speed limits that ensure safe navigation around curves. The radius of curvature (R) plays a crucial role in defining the maximum safe velocity: tighter curves require lower speed limits, while flatter curves may allow higher speeds, striking a balance between safety and traffic efficiency.

Moreover, μ represents the road surface's ability to provide traction, directly influencing the maximum safe velocity. To optimize road safety, proper road maintenance and the selection of appropriate road materials are essential to enhance frictional properties. The value of g is 9.8 m s^{-2}. The values for μ in different traffic conditions are given in Table 1. It is worth noting that the values presented in 1 are sourced from existing literature. These values are typically obtained through testing and analysis specific to the site. However, for our study, we rely on values reported in the literature (Younes, 2023; Kordani et al., 2018). Our focus is on assessing the practical application of NHSRM, particularly in predicting outcomes under challenging weather conditions.

In any traffic condition, the fitting of Eq. (6) to real data plays a vital role. v_f in Eq. (6) corresponds to free flow velocity. This velocity varies according to different traffic conditions. It is impacted by the geometry of a highway, weather conditions, and driver characteristics. In adverse traffic conditions, this velocity can be modeled as Eq. (7), and thus it is employed directly in the velocity–density relationship to account for the impacts of various weather conditions. Next, we demonstrate how the dynamics in the Fundamental Diagram (FD) of traffic vary according to different weather conditions.

3.2.1. The fundamental diagram of traffic

Traffic flow, q, is the fundamental relation between ρ and v, which is

$$q = \rho v, \tag{8}$$

where v is $V(\rho)$ which is given by Eq. (6). Thus, q is represented as $q(\rho)$, and it is computed as

$$q(\rho) = \rho V(\rho). \tag{9}$$

The FD results from Eq. (9) are shown in Figs. 2 and 3 for dry pavement, light rainfall, moderate rainfall and heavy rainfall, when R is 120 m and 500 m, respectively. The ranges for μ are given in Table 1. The ρ_{cr} is 18 veh/km while the maximum density (ρ_m) is 83 veh/km. For a curve with $R = 120$ m, μ for dry pavement is 0.75, while the capacity is 707 veh/h. During light rainfall, μ is 0.55, while the capacity reduces to 606 veh/h. Whereas in moderate and heavy rainfall, μ ranges from 0.40 to 0.20, while the capacity significantly reduces to 447 veh/h and 258 veh/h. In general, 63.50% reduction in the capacity of traffic is observed.

The results of curve with $R = 500$ m are shown in Fig. 3 for μ is 0.75, while the traffic capacity is 963 veh/h. During light rainfall, μ is 0.55, while the capacity reduces to 790 veh/h. Whereas in moderate and heavy rainfall, μ ranges from 0.40 to 0.20, and the capacity significantly reduces to 659 veh/h and 571 veh/h. A reduction of 40.70% in traffic capacity is observed. This information is employed for weather conditions in Eq. (7) to obtain v_s approximated as v_f, and consequently employed in Eq. (6) to perform investigations.

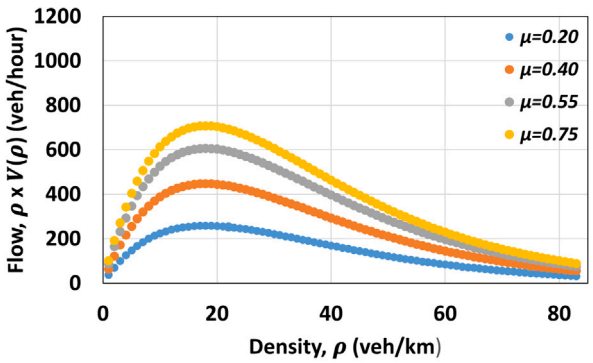

Fig. 2. The flow-density relationship subjected to assorted μ during various traffic conditions with $R = 120$ m.

3.2.2. The critical role of the fundamental diagram of traffic

In Section 3.2.1, we have demonstrated (see Figs. 2 and 3), the variations in the FD between flow and density with different values of μ. This FD of traffic is vital for the output of any model, thus, it plays a critical role in the predictions. Given the NHRSM, the key points gained from the previous illustrations are;

- The primary feature of the FD is its ability to graphically illustrate the dynamic relation between traffic density and flow. Macroscopic continuum models in general provide an effective tool for accurately representing real-world traffic phenomena by incorporating the insights gained from the FD into the simulations. This inclusion enables the simulations to accurately represent situations ranging from equilibrium conditions, when a particular density correlates to flow, to the domain of non-equilibrium circumstances, where different flows can coexist for a specified density range.
- The FD serves as a pinning point for the simulations when incorporated with the NHSRM. It guarantees that the simulated traffic patterns follow the fundamental rules governing traffic behavior. Thus, given traffic conditions are accurately captured by the FD following an appropriate methodology and theoretical background, the NHSRM results in precise predictions. As previously, the v_f is designed based on the criteria suggested by AASHTO (AASHTO, 2011), subsequently, the NHSRM will efficiently and more realistically simulate different traffic conditions.

3.3. Environment

In this study, a speculative highway of 10,000 m is considered with a specific focus on a sharp curve that is located between 5500 m and 6500 m. The Radius of curvature is 120 m and 500 m, while traffic conditions are observed for 3600 s. Additionally, to implement the NHSRM on this highway, the model is first discretized in space and time using the First ORder CEntered (FORCE) technique (Khan et al., 2020) . This technique is further elaborated in Section 3.4. The model's stability is ensured by employing the Courant, Friedrich, and Lewy (CFL) (Moura and Kubrusly, 2012; Imran et al., 2024) conditions. For NHSRM, the road step is $\Delta x = 200$ m, and the time step is $\Delta t = 1$ s. The total simulation time is 3600 s. The maximum velocity is $v_f = 30$ m/s over the straight section, while that on the curved section is Eq. (7) and the

Table 1
Coefficient of friction μ for different weather conditions (Younes, 2023; Kordani et al., 2018).

Description	Range
Dry pavement	0.7–0.9
Light rainfall	0.5–0.7
Moderate rainfall	0.2–0.5
Heavy rainfall	<0.2
Snow	0.1–0.4

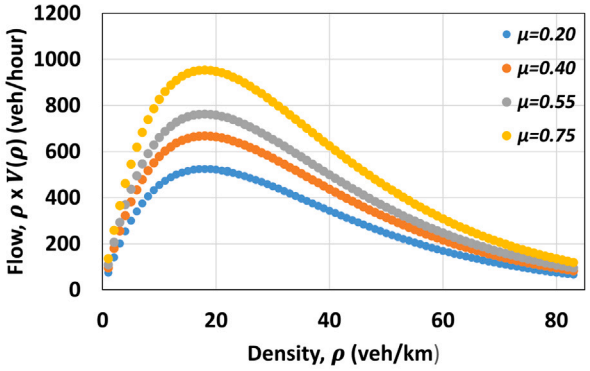

Fig. 3. The flow-density relationship subjected to assorted μ during various traffic conditions with $R = 500$ m.

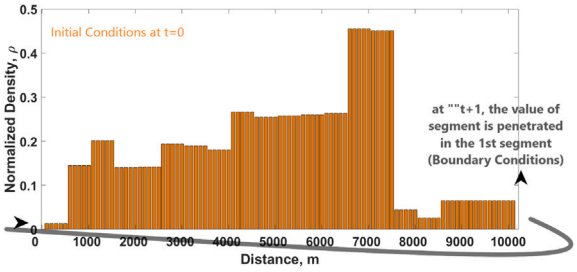

Fig. 4. Illustration of initial and boundary conditions over the 10,000 m highway.

maximum normalized density is $\rho_m = 1$. τ_r ranges between 0.8 s to 1.0 s, and τ_b ranges between 0.1 s and 0.2 s (Basak et al., 2013; Ping et al., 2004). The maximum deceleration is 7 ms^{-2} (Qu et al., 2014). The initial density at time $t = 0$, and the boundary conditions at time $t+1$ are illustrated in Fig. 4. These conditions are attributed to circular road conditions.

Circular traffic conditions are commonly used in MATLAB simulations for traffic flow models due to their closed-loop nature, eliminating the need for explicit endpoints and avoiding boundary effects. This setup ensures a consistent, uninterrupted traffic flow, simplifying the modeling process. The closed-loop geometry is particularly useful for studying wave propagation and congestion patterns, making it easier to analyze disturbances in traffic flow. Additionally, circular conditions provide a simplified visualization of continuous traffic, facilitating the interpretation of simulation results. The choice of circular conditions reflects a balance between modeling simplicity and the ability to capture essential features of traffic dynamics.

3.4. Hyperbolocity and numerical technique for the NHSRM decomposition

The NHSRM is decomposed employing the FORCE technique. A conserved form of a traffic system is given by

$$\beta_t + f(\beta)_x = S(\beta), \tag{10}$$

The subscripts, t and x represent temporal and spatial derivatives, respectively. The NHSRM in conserved form is

$$\beta = \begin{pmatrix} \rho \\ \rho v \end{pmatrix}, f(\beta) = \begin{pmatrix} \rho v \\ \frac{(\rho v)^2}{\rho} + f\varsigma\rho \end{pmatrix}, \quad S(\beta) = \begin{pmatrix} 0 \\ \rho\frac{V(\rho)-v}{\tau} \end{pmatrix}. \tag{11}$$

The traffic system in quasilinear form is

$$\beta_t + A(\beta)\beta_x = 0, \tag{12}$$

where the Jacobian matrix is $A(\beta)$, it holds the gradients of the functions of variables. The Jacobian matrix for the NHSRM is

$$A(\beta) = \begin{pmatrix} 0 & 1 \\ -v^2 + f\varsigma & 2v \end{pmatrix}, \tag{13}$$

and the eigenvalues are the solutions of

$$|A(\beta) - \lambda I| = \begin{vmatrix} -\lambda & 1 \\ -v^2 + f\varsigma & 2v - \lambda \end{vmatrix}, \tag{14}$$

which are

$$\lambda_1 = v + \sqrt{f\varsigma}, \lambda_2 = v - \sqrt{f\varsigma}, \tag{15}$$

where

$$\sqrt{f\varsigma} = \sqrt{\left(\frac{|V(\rho) - v|}{v \times (\tau_r + \tau_b) + \frac{v^2}{2a_m}}\right)\frac{b_a}{b_m}}. \tag{16}$$

The NHSRM is hyperbolic as the eigenvalues are real and distinct. During congestion, the variations in flow occur at λ_2 (below average velocity), while during free flow occur at λ_1 (higher speeds).

To numerically solve the NHSRM, let x_M be the road length with M equidistant segments, thus, the length of each segment is $\Delta x = x_m/M$. Let t_N be the total time with N time steps so a time step is $\Delta t = t_N/N$ given by $t_{n+1} - t_n$. β and $f(\beta)$ are computed (approximated) for the segments $(x_i + \frac{\Delta x}{2}, x_i - \frac{\Delta x}{2})$, and the data variables are obtained for each of the M segments for time (t_{n+1}, t_n).

The FORCE technique is now employed to approximate flow at the road segment boundaries (Toro et al., 1996) This technique combines the first-order Lax–Friedrichs scheme (Al-nasur et al., 2008) with the second-order Richtmyer scheme (Richtmyer, 1957). The average values of the data variables are β_i in the ith segment. The change in traffic density and flow at the segment boundary is approximated by the flux. With the Lax–Friedrichs scheme, the flux at the boundary of segments i and $i+1$ in the nth time step is given by

$$(f^n_{i+\frac{1}{2}}(\beta^n_i, \beta^n_{i+1}))^l = \frac{1}{2}\left(f(\beta^n_i) + f(\beta^n_{i+1})\right) + \frac{1}{2}\frac{\Delta t}{\Delta x}\left(\beta^n_i - \beta^n_{i+1}\right), \tag{17}$$

where $f(\beta^n_i)$ and $f(\beta^n_{i+1})$ are the corresponding values of the functions of the data variables in segments i and $i+1$, respectively. The superscript l denotes the Lax–Friedrichs scheme. The data variables obtained with the Richtmyer scheme are (Richtmyer, 1957)

$$\beta^n_{i+\frac{1}{2}} = \frac{1}{2}\left(\beta^n_i + \beta^n_{i+1}\right) + \frac{1}{2}\frac{\Delta t}{\Delta x}\left(f(\beta^n_i) - f(\beta^n_{i+1})\right), \tag{18}$$

Table 2
Simulation parameters.

Description	Value
Simulation time	3,600 s
Highway length	10,000 m
v_f (straight section)	30 m/s
v_f (curved section)	Eq. (7)
Δt	1 s
Δx	200 m
τ	15 s
τ_r	0.9 s
τ_b	0.2 s
$V(\rho)$	Eq. (6)
ρ_m	1
R	120 m and 500 m
g	9.8 m s^{-2}
μ	0.75, 0.55, 0.40 and 0.20
a_m	7 m s^{-2}

and the corresponding flux is

$$(f^n_{i+\frac{1}{2}}(\beta^n_i, \beta^n_{i+1}))^r = f(\beta^n_{i+\frac{1}{2}}), \tag{19}$$

where the superscript r denotes the Richtmyer scheme. The flux at the segment boundaries is obtained by averaging Eqs. (17) and (19) obtained from the Lax–Friedrichs and Richtmyer schemes, respectively, which gives

$$f^{n+1}_i = \frac{1}{2}\left((f^n_{i+\frac{1}{2}})^r + (f^n_{i+\frac{1}{2}})^l\right). \tag{20}$$

This approximates the change in density and flow without considering the source. The source terms of the NHSRM is

$$S(\beta^n_i) = \left(\frac{V(\rho^n_i) - v^n_i}{\tau}\right). \tag{21}$$

The updated data variables are obtained by including the source term which gives

$$\beta^{n+1}_i = \beta^n_i - \frac{\Delta t}{\Delta x}\left(f^n_{i+\frac{1}{2}} - f^n_{i-\frac{1}{2}}\right) + \Delta t S(\beta^n_i). \tag{22}$$

4. Results

In this Section, the results of the study are briefly presented. The simulation parameters are given in Table 2. The spatio-temporal evolution of velocity and density is analyzed, which provides deeper insights into the velocity breakdowns and density shockwave formation and dissipation. Additionally, the impact of rainfall intensity and R of curve on the Segment Travel Time (S_{TT}) (Afrin and Yodo, 2020) is assessed, which is computed as

$$S^n_{TTi} = \frac{L_i}{v^n_i}, \tag{23}$$

where the subscripts i and n are space and time indices, L_i is the segment length and v^n_i is the velocity of segment i at time n.

4.1. Analysis of the travel time and spatiotemporal evolution of velocity and density on dry pavement ($\mu = 0.75$)

4.1.1. Traffic insights with curve $R = 120$ m

The spatiotemporal evolution of velocity over the 10,000 m highway for 3600 s, considering a friction coefficient $\mu = 0.75$ and radius of curvature $R = 120$ m is illustrated in Fig. 5. Initially, the formation of a shockwave is observed, originating between 6800 m and 7800 m, which subsequently spills back over time. Noteworthy, the sharp curve between 5500 m and 6500 m has minimal impact on the velocity dynamics in dry weather conditions. The velocity remains smooth and steady at 14.0 m/s, except for the initial shockwave, while low velocities occur mainly due to the initial and boundary conditions provided to the model. This critical scenario allows us to exercise the worst traffic flow conditions to gain valuable insights, such as the formation and propagation of the velocity and density shockwave.

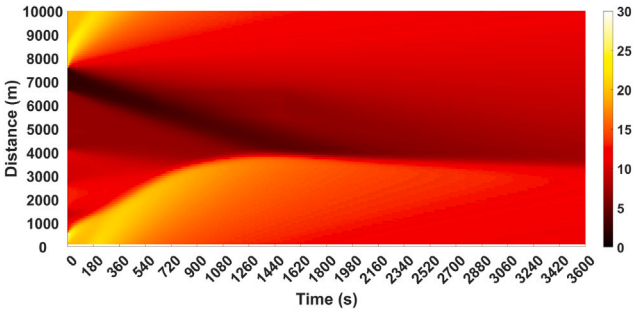

Fig. 5. Spatiotemporal evolution of velocity over the 10,000 m highway for 3600 s with $\mu = 0.75$ and R = 120 m.

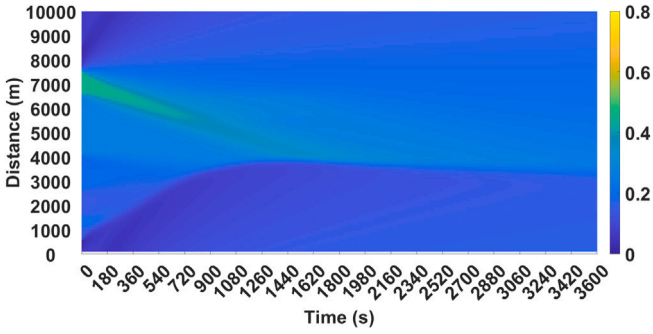

Fig. 6. Spatiotemporal evolution of density over the 10,000 m highway for 3600 s with $\mu = 0.75$ and $R = 120$ m.

Density shockwave analysis are performed to further elaborate the results of this study. Fig. 6 shows the evolution of density over the 10,000 m highway with a curve of $R = 120$ m and $\mu = 0.75$, representing dry pavement conditions. The initial density shockwave resulted from an inactive bottleneck propagating backward, which meets another density shockwave relatively very small, due to the curved section between 5500 m and 6500 m at 600 s into the analysis. In this scenario, the curve has little impact on the propagation of the density shockwave and the upstream. However, a visible shockwave formation is observed, providing significant insights into traffic dynamics over the highway.

Moreover, the travel time contour plot with $\mu = 0.75$ and $R = 120$ m is shown in Fig. 7. At first, the travel time elevates due to the spillback effect of the velocity shockwave, it is as high as 80 s for certain segments. Further, with the dissipation of the shockwave, the travel time reduces to 30 s, demonstrating the dynamic behavior of the traffic flow. The dry pavement conditions play a significant role in minimizing the impact of the sharp curve between positions 5500 m and 6500 m on the travel time. This analysis of velocity, density, and travel time for $\mu = 0.75$ provides insights and understanding of critical traffic scenarios. Understanding the dynamics of traffic in different weather conditions is vital for enhancing traffic management strategies, thus we consider this scenario as the base scenario for comparative analysis with other traffic conditions.

4.1.2. Traffic insights with curve $R = 500$ m

The spatiotemporal evolution of velocity over the 10,000 m highway for 3600 s, considering a friction coefficient $\mu = 0.75$ and radius of curvature $R = 500$ m is illustrated in Fig. 8. At the outset, the formation of the shockwave is observed, but in this scenario, the formation of the shockwave is for a shorter time compared to the previous scenario.

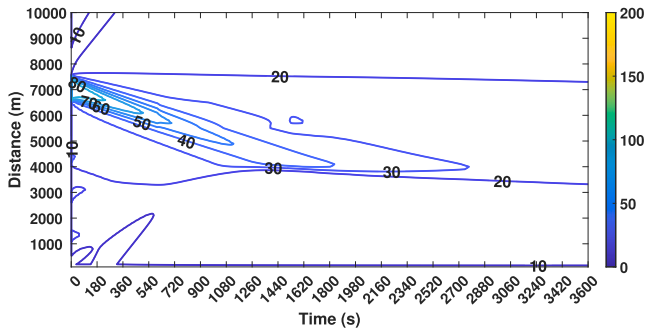

Fig. 7. Contour of the total travel time of traffic over the 10,000 m highway for 3600 s with $\mu = 0.75$ and R = 120 m.

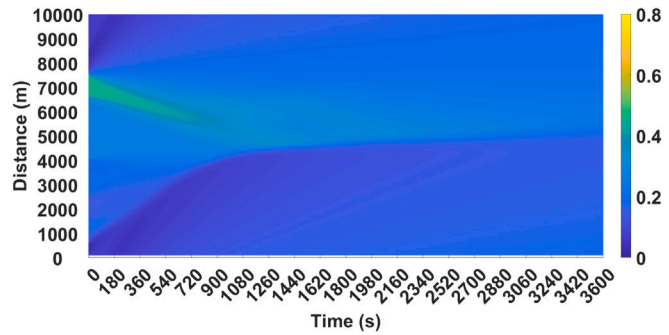

Fig. 9. Spatiotemporal evolution of density over the 10,000 m highway for 3600 s with $\mu = 0.75$ and $R = 500$ m.

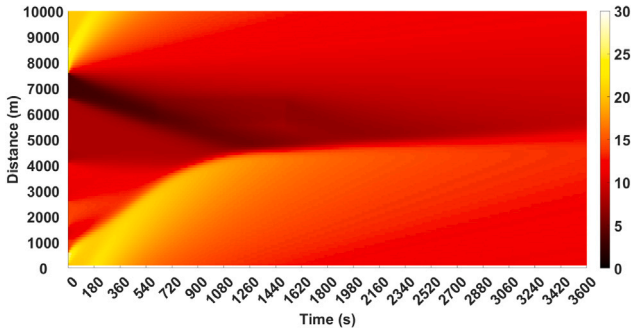

Fig. 8. Spatiotemporal evolution of velocity over the 10,000 m highway for 3600 s with $\mu = 0.75$ and $R = 500$ m.

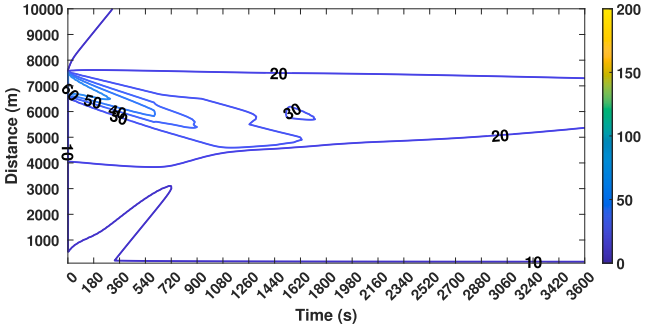

Fig. 10. Contour of the total travel time of traffic over the 10,000 m highway for 3600 s with $\mu = 0.75$ and $R = 500$ m.

It is observable that the shockwave dissipates faster, and the velocity breakdowns are minimal at the curve due to the larger radius of the curve. The velocity evolution is smoother, and the impact of the curve on upstream traffic is not significant.

The evolution of density over the 10,000 m highway with a curve of $R = 500$ m and $\mu = 0.75$ for 3600 s is shown in Fig. 9. The initial density shockwave resulted from an inactive bottleneck propagating backward, which meets another density shockwave relatively smaller than that with the curve of $R = 120$ m, due to the curved section between 5500 m and 6500 m at 600 s into the analysis. However, the shockwave formation and propagation time is smaller, and after 1200 s into the analysis, the density evolution is smoother.

The travel time contour plot with $\mu = 0.75$ and $R = 500$ m is shown in Fig. 10. At first, the travel time elevates due to the spillback effect of the velocity shockwave, it is as high as 60 s for certain segments, however, it is less than the previous scenario. Further, with the dissipation of the shockwave, the travel time reduces to 30 s sooner. The larger radius significantly reduces the travel time over the curve. The dissipation of shockwave initiates as soon as 1070 s into the analysis, which is small compared to the previous scenario.

4.2. Analysis of the travel time and spatiotemporal evolution of velocity and density during light rainfall, $\mu = 0.55$

4.2.1. Traffic insights with curve $R = 120$ m

The spatiotemporal evolution of velocity over a 10,000 m highway, for a duration of 3600 s, with $\mu = 0.55$ and $R = 120$ m is presented in Fig. 11. Initially, a noticeable shockwave emerges, originating between 6800 m and 7800 m. This shockwave propagates backward over time. Moreover, between 5500 m and 6500 m, we observe velocity breakdowns resulting from light rainfall and the geometric characteristics of the highway. Around 600 s into the analysis, the development of another shockwave is observed, originating between 5500 m and 6500 m. This second shockwave eventually merges with the existing one, consequently, further impacting the velocity behavior upstream. In all, the average velocity of the highway experiences a decline, it is 11.0 m/s. This decline in average velocity is vital to understand.

The evolution of density over the 10,000 m highway with a curve of $R = 120$ m and $\mu = 0.55$ for 3600 s is shown in Fig. 12. The initial density shockwave resulted from an inactive bottleneck propagating backward, which meets another density shockwave, due to the curved section between 5500 m and 6500 m at 600 s and beyond into the analysis. The formation time of the shockwave and the backward propagation increases. The upstream traffic conditions are more denser due to the intensity of the rainfall over the curve.

The travel time contour with $\mu = 0.55$ and $R = 120$ m is shown in Fig. 13. Initially, the travel time exhibits an elevation because of the spillback effect caused by the velocity shockwave. Noteworthy, the contours are stretched compared to the previous scenario, signifying higher travel times across the entire time horizon. A vital observation is the presence of an evident contour representing a travel time of 80 s between 5500 m and 6500 m at approximately 600 seconds into the analysis. It is evident from the results that under the influence of light rainfall, the overall performance encounters deterioration, indicating a reduction in the overall efficiency of traffic flow during light rainfall. The travel time contour for $\mu = 0.55$ provides valuable insights into the temporal variations of travel time along the highway. The presence of distinct features and variations highlights the importance of considering different factors and their effects on traffic flow for efficient transportation management.

4.2.2. Traffic insights with curve $R = 500$ m

The spatiotemporal evolution of velocity over a 10,000 m highway, for a duration of 3600 s, with $\mu = 0.55$ and $R = 500$ m is presented in Fig. 14. The initial dynamics of both scenarios are similar, however, over time with the larger curve the velocity evolution is smoother. There are no breakdowns, and it is evident that the intensity of rainfall

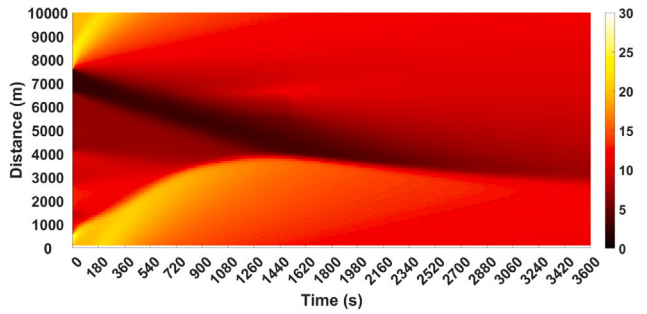

Fig. 11. Spatiotemporal evolution of velocity over the 10,000 m highway for 3600 s with $\mu = 0.55$ and $R = 120$ m.

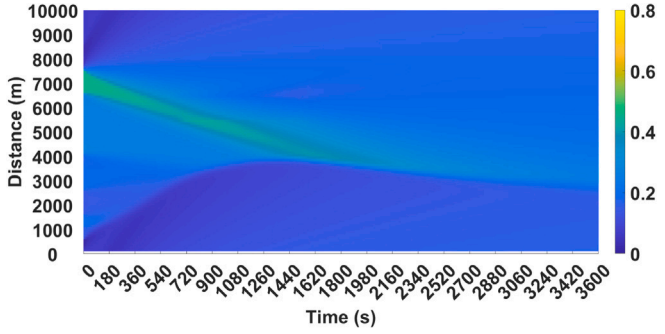

Fig. 12. Spatiotemporal evolution of density over the 10,000 m highway for 3600 s with $\mu = 0.55$ and $R = 120$ m.

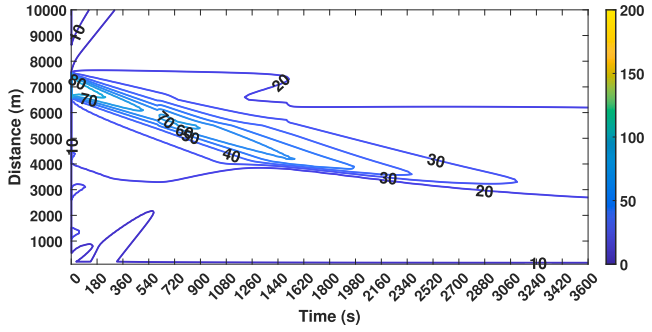

Fig. 13. Contour of the total travel time of traffic over the 10,000 m highway for 3600 s with $\mu = 0.55$ and $R = 120$ m.

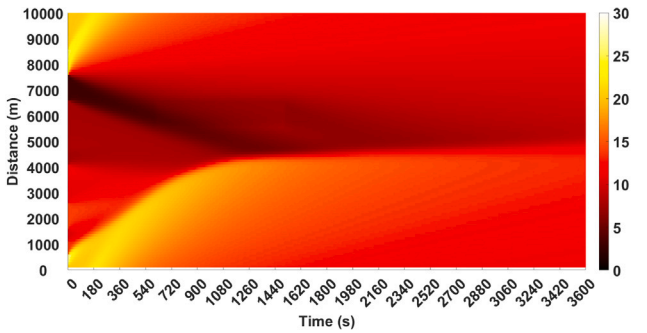

Fig. 14. Spatiotemporal evolution of velocity over the 10,000 m highway for 3600 s with $\mu = 0.55$ and $R = 500$ m.

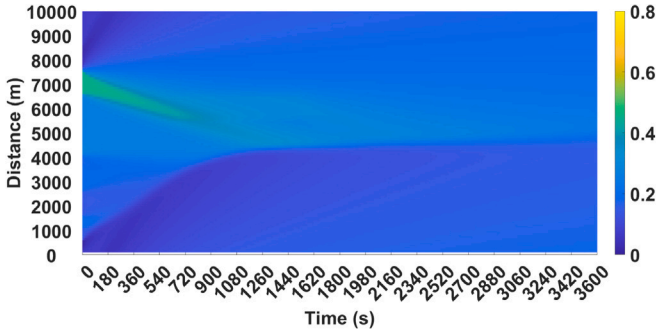

Fig. 15. Spatiotemporal evolution of density over the 10,000 m highway for 3600 s with $\mu = 0.55$ and $R = 500$ m.

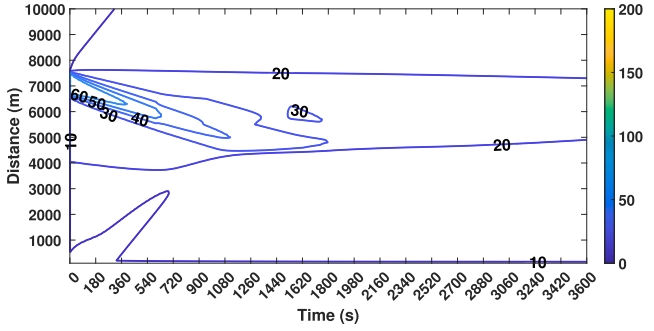

Fig. 16. Contour of the total travel time of traffic over the 10,000 m highway for 3600 s with $\mu = 0.55$ and $R = 500$ m.

has little to no impact on the velocity evolution. The shockwave dissipation is faster and the rainfall over the curve has no significant impact which is due to the larger radius of the curve.

The evolution of density over the 10,000 m highway with a curve of $R = 500$ m and $\mu = 0.55$ for 3600 s is shown in Fig. 15. The initial density shockwave resulted from an inactive bottleneck propagating backward, which meets another density shockwave, due to the curve of $R = 500$ m between 5500 m and 6500 m at 600 s and beyond into the analysis. The formation time of the shockwave and the backward propagation increases compared to that on dry pavement. The upstream density evolution is impacted and is slower.

The travel time contour with $\mu = 0.55$ and $R = 500$ m is shown in Fig. 16. Initially, the travel time exhibits an elevation because of the spillback effect caused by the velocity shockwave. The maximum segment travel time observed is 60 s, which eventually reduces to 20 s over time. Due to faster velocity evolution, the travel time is significantly reduced. With $R = 120$ m, the maximum travel time observed was 80 s, while with $R = 500$ m, this time is 60 s. Moreover, the travel time is reduced very soon and uniform travel time is observed later in the analysis.

4.3. Analysis of the travel time and spatiotemporal evolution of velocity and density during moderate rainfall, $\mu = 0.40$

4.3.1. Traffic insights with curve $R = 120$ m

The spatiotemporal evolution of velocity over a 10,000 m highway with $\mu = 0.40$ and $R = 120$ m for 3600 s is presented in Fig. 17 for moderate rainfall. At the outset, an evident shockwave emerges, originating between 6800 m and 7800 m. This shockwave propagates backward over the time horizon. Moreover, between 5500 m and 6500 m, we observe sharp velocity breakdowns resulting from the high intensity of the rainfall (moderate rainfall) and the geometric characteristics of the highway. Around 600 s into the analysis, another shockwave is observed, originating between 5500 m and 6500 m. This second shockwave eventually merges with the existing one, consequently,

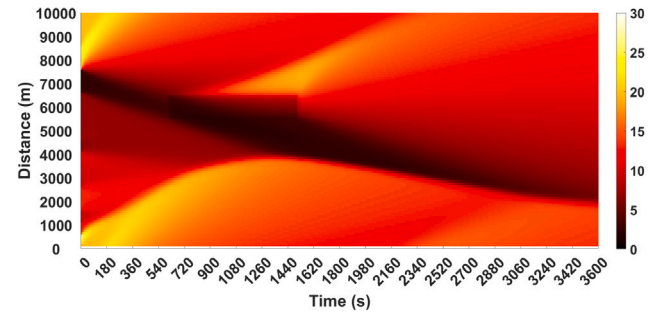

Fig. 17. Spatiotemporal evolution of velocity over the 10,000 m highway for 3600 s with $\mu = 0.40$ and $R = 120$ m.

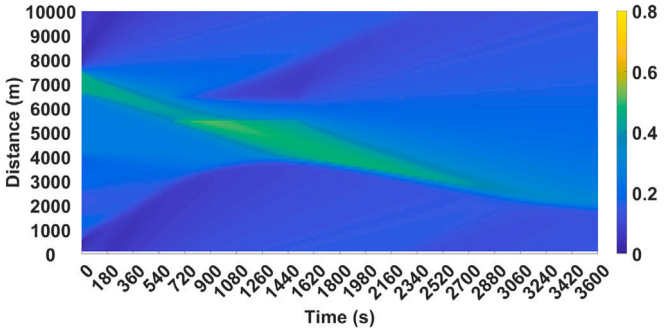

Fig. 18. Spatiotemporal evolution of density over the 10,000 m highway for 3600 s with $\mu = 0.40$ and $R = 120$ m.

further severely impacting the velocity behavior upstream, while the average velocity of the highway experiences a decline, it is 9.1 m/s.

The evolution of density over the 10,000 m highway with a curve of $R = 120$ m and $\mu = 0.40$ for 3600 s is shown in Fig. 18. The initial density shockwave resulted from an inactive bottleneck propagating backward, which meets another density shockwave, due to the curved section between 5500 m and 6500 m at 600 s and beyond into the analysis. In this scenario, the intensity of the rainfall has a stronger effect. The traffic on the curve becomes more congested, and the congestion from the rainfall lasts longer. The density evolution is not smooth, and the rainfall, combined with the sharp curve, has a greater impact upstream.

The contour of travel time with $\mu = 0.40$ and $R = 120$ m is shown in Fig. 19. Initially, the travel time exhibits an elevation because of the spillback effect caused by the velocity shockwave. Noticeably, the contours are further stretched compared to the previous scenarios. It signifies higher travel times across the entire time horizon. A vital observation is the presence of an evident contour representing a travel time of 110 s between 5500 m and 6500 m at approximately 600 seconds into the analysis. It is evident from the results that under the influence of moderate rainfall, the overall performance encounters deterioration, indicating a reduction in the overall efficiency of traffic flow during light rainfall.

4.3.2. *Traffic insights with curve $R = 500$ m*

The spatiotemporal evolution of velocity over a 10,000 m highway with $\mu = 0.40$ and $R = 500$ m for 3600 s is presented in Fig. 20 for moderate rainfall. The velocity evolution is smoother, and the impact of rainfall is vital in this case. Compared to the previous scenario, the impact is smaller, but the velocity drop is significant over the curve. The velocity evolution is slightly timid compared to $\mu = 0.55$. The formation time of the shockwave slightly increases.

The evolution of density over the 10,000 m highway with a curve of $R = 500$ m and $\mu = 0.40$ for 3600 s is shown in Fig. 21. The initial

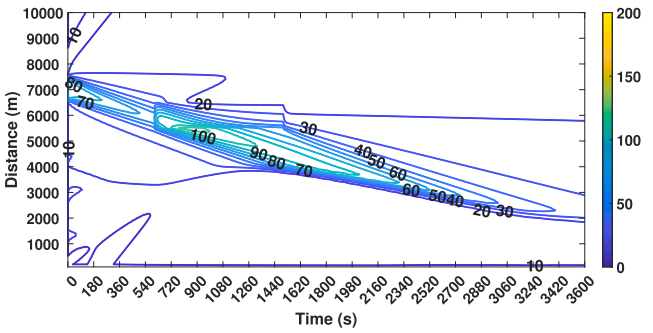

Fig. 19. Contour of the total travel time of traffic over the 10,000 m highway for 3600 s with $\mu = 0.40$ and $R = 120$ m.

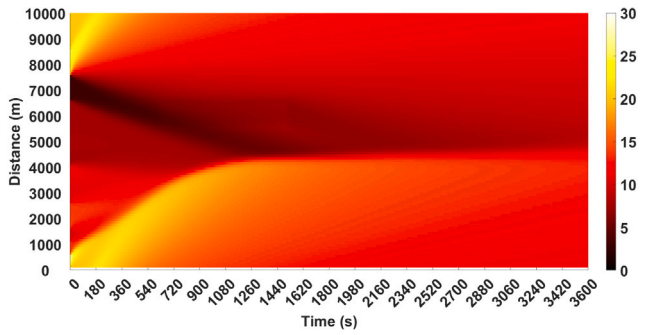

Fig. 20. Spatiotemporal evolution of velocity over the 10,000 m highway for 3600 s with $\mu = 0.40$ and $R = 500$ m.

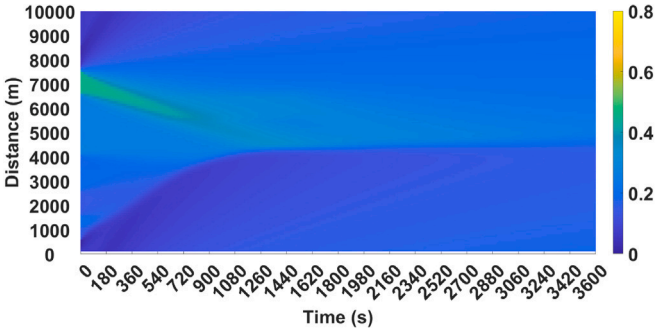

Fig. 21. Spatiotemporal evolution of density over the 10,000 m highway for 3600 s with $\mu = 0.40$ and $R = 500$ m.

density shockwave resulted from an inactive bottleneck propagating backward, which meets another density shockwave, due to the curved section between 5500 m and 6500 m at 600 s and beyond into the analysis. When $R = 500$ m, the rainfall intensity does not have a severe impact, and there are slight changes in the density shockwave evolution compared to evolution with $\mu = 0.55$. Nevertheless, a noticeable traffic jam forms on the curve, affecting the traffic flow upstream.

The contour of travel time with $\mu = 0.40$ and $R = 500$ m is shown in Fig. 22. Initially, the travel time exhibits an elevation because of the spillback effect caused by the velocity shockwave. Noticeably, the contours are further stretched compared to the previous scenarios. It signifies higher travel times across the entire time horizon. However, the maximum travel time is observed to be 60 s, which is significantly smaller than the scenario with curve $R = 120$ m.

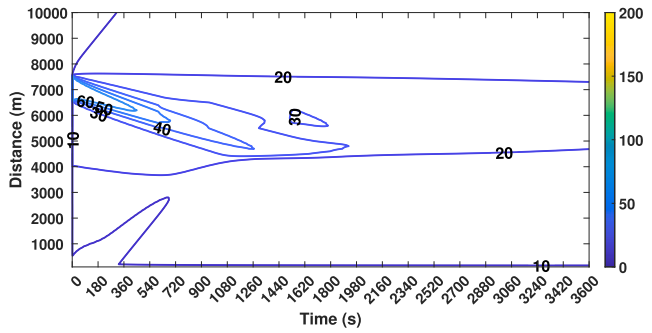

Fig. 22. Contour of the total travel time of traffic over the 10,000 m highway for 3600 s with $\mu = 0.40$ and $R = 500$ m.

4.4. Analysis of the travel time and spatiotemporal evolution of velocity and density during heavy rainfall, $\mu = 0.20$

4.4.1. Traffic insights with curve $R = 120$ m

The spatiotemporal evolution of velocity over a 10,000 m highway with $\mu = 0.20$ and $R = 120$ s for 3600 s is presented in Fig. 23 for heavy rainfall. Initially, a shockwave emerges, originating between 6800 m and 7800 m. This shockwave propagates backward over time. Moreover, between 5500 m and 6500 m, we observe extremely sharp velocity breakdowns resulting from the high intensity of the rainfall (heavy rainfall) and the geometric characteristics of the highway. Around 600 s into the analysis, another shockwave is observed, originating between 5500 m and 6500 m. This second shockwave eventually merges with the existing one, consequently, further severely impacting the velocity behavior upstream, while the average velocity of the highway experiences a decline, it is 7.2 m/s, while the limited flow is observed downstream due to the jam over the curve. The downstream traffic foresees light traffic conditions, thus resulting in smoother flows, but a deteriorating situation over the curve is observed, which is jam traffic conditions for a longer time upstream.

The evolution of density over the 10,000 m highway with a curve of $R = 120$ m and $\mu = 0.20$ for 3600 s is shown in Fig. 24. The initial density shockwave resulted from an inactive bottleneck propagating backward, which meets another density shockwave, due to the curved section between 5500 m and 6500 m at 600 s and beyond into the analysis. In this scenario, a traffic jam occurs upstream of the curve. The curve restricts incoming traffic due to heavy rainfall, leading to a prolonged jam. On the contrary, downstream traffic flows more smoothly due to limited outflow from the curve, but chaotic conditions persist due to intense rainfall effects. The density evolution upstream is both timid and disorderly.

The contour of travel time with $\mu = 0.20$ and $R = 120$ m is shown in Fig. 25. The travel time exhibits an elevation because of the spillback effect caused by the velocity shockwave. Noticeably, the contours are further stretched compared to the previous scenarios. It signifies higher travel times across the entire time horizon. A vital observation is the presence of an evident contour representing a travel time of 200 s between 5500 m and 6500 m at approximately 600 seconds into the analysis. It is evident from the results that under the influence of heavy rainfall, the overall performance encounters deterioration, indicating a reduction in the overall efficiency of traffic flow during rainfall.

4.4.2. Traffic insights with curve $R = 500$ m

The spatiotemporal evolution of velocity over a 10,000 m highway with $\mu = 0.20$ and $R = 500$ s for 3600 s is presented in Fig. 26 for heavy rainfall. Initially, a shockwave emerges, originating between 6800 m and 7800 m. This shockwave propagates backward over the time horizon. In this scenario, vital changes are observed. Over the curve, velocity declines due to the intensity of the rainfall, however, compared

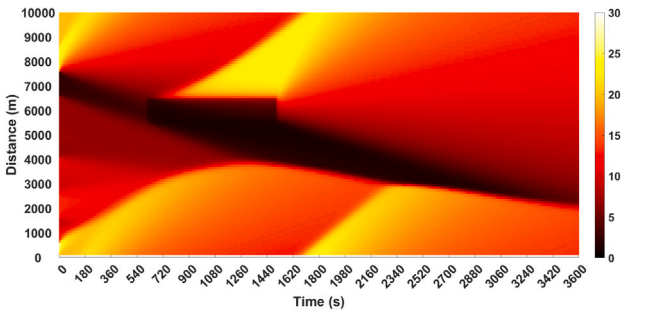

Fig. 23. Spatiotemporal evolution of velocity over the 10,000 m highway for 3600 s with $\mu = 0.20$ and $R = 120$ m.

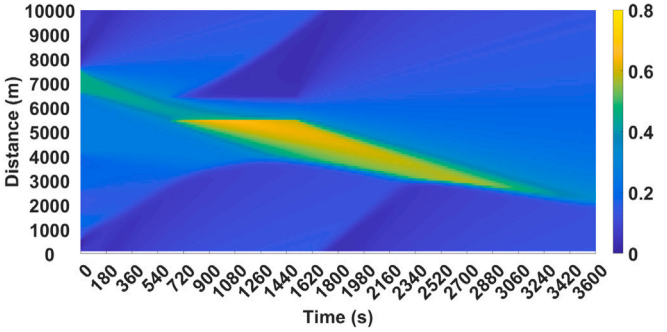

Fig. 24. Spatiotemporal evolution of density over the 10,000 m highway for 3600 s with $\mu = 0.20$ and $R = 120$ m.

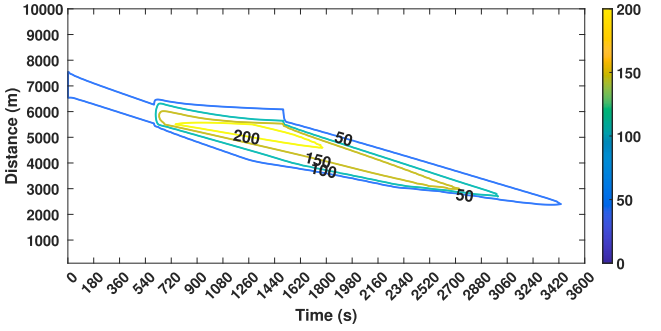

Fig. 25. Contour of the total travel time of traffic over the 10000 m highway for 3600 s with $\mu = 0.20$ and $R = 120$ m.

to the highway with the curve of $R = 120$ m, the changes are less significant. Further, with other intensities of the rainfall, the velocity evolution is smoother, but in this scenario, the velocity evolution is more timid and the breakdowns are significant.

The evolution of density over the 10,000 m highway with a curve of $R = 500$ m and $\mu = 0.20$ for 3600 s is shown in Fig. 27. The initial density shockwave resulted from an inactive bottleneck propagating backward, which meets another density shockwave, due to the curved section between 5500 m and 6500 m at 600 s and beyond into the analysis. In this situation, traffic upstream of the curve experiences an impact with $R = 500$ m. There is a noticeable increase in the time it takes for the jam to form and spread backward. Additionally, the density rises upstream of the curve, leading to a less smooth density evolution. The dissipation time of the shockwave also increases in this scenario. However, when compared to the results with $R = 120$ m, the density evolution is relatively smoother. Rainfall intensity, however, has a significant impact on jam formation and the backward propagation of the density shockwave.

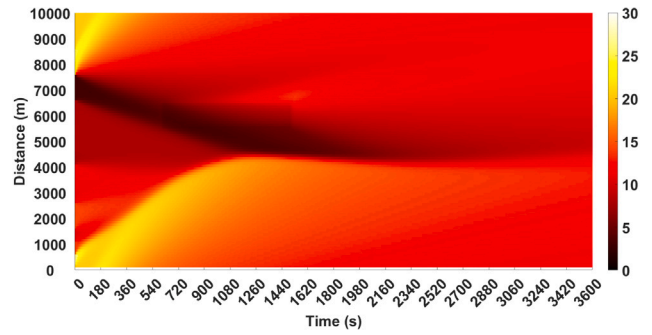

Fig. 26. Spatiotemporal evolution of velocity over the 10,000 m highway for 3600 s with $\mu = 0.20$ and $R = 500$ m.

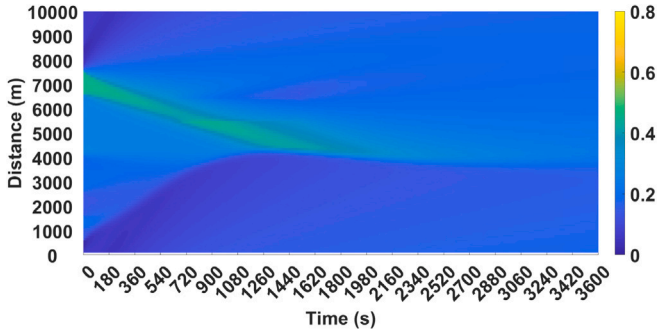

Fig. 27. Spatiotemporal evolution of density over the 10,000 m highway for 3600 s with $\mu = 0.20$ and $R = 500$ m.

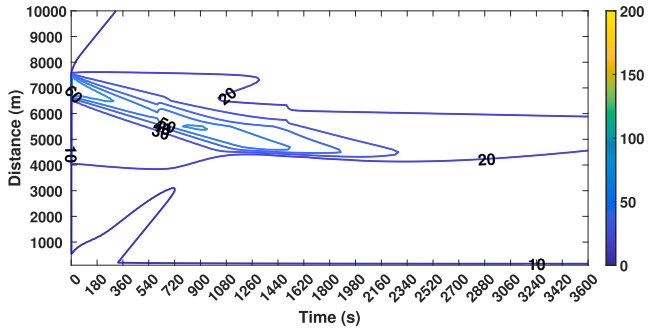

Fig. 28. Contour of the total travel time of traffic over the 10000 m highway for 3600 s with $\mu = 0.20$ and $R = 500$ m.

The contour of travel time with $\mu = 0.20$ and $R = 500$ m is shown in Fig. 28. The travel time exhibits an elevation because of the spillback effect caused by the velocity shockwave. Noticeably, the contours are further stretched compared to the previous scenarios. It signifies higher travel times across the entire time horizon. The maximum travel time for certain segments is 60 s, due to the larger radius of the curve the segment travel time remains the same. However, with the increase in the shockwave formation time, longer segment travel times are evident.

4.5. Analysis of the variance of velocity subject to assorted values of μ

The variance in velocity during different weather conditions with curve $R = 120$ m is shown in Fig. 29. During dry weather conditions with $\mu = 0.75$, it is observable that the variance in velocity is relatively smaller. With $\mu = 0.55$, the differences in velocity variance are observed to be minimal compared to the first scenario with $\mu = 0.75$. As the μ is decreased to 0.40 moderate rainfall, the variance in the velocity is significant. It is evident that changes in traffic occur at 600 s in the

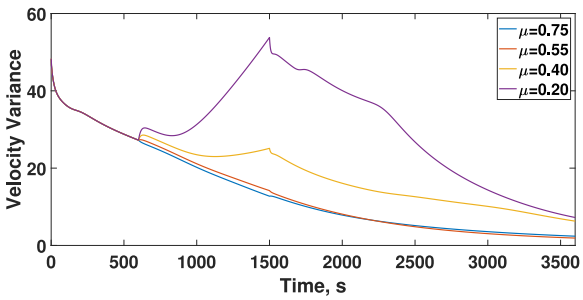

Fig. 29. Variance of velocity during different weather conditions with $R = 120$ m.

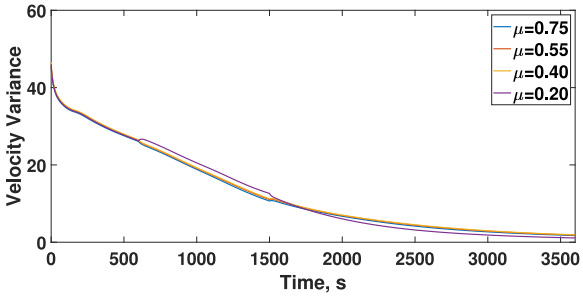

Fig. 30. Variance of velocity during different weather conditions with $R = 500$ m.

simulations, but the variance in velocity increase later in time. This is because of the impacts of changes in traffic at one point, and these changes signify over the upstream with time. Similarly, with $\mu = 0.20$, the variance in velocity is significantly large. The variance in velocity after 600 s into the analysis signifies to a greater extent.

The variance of velocity of curve with $R = 500$ m is shown in Fig. 30. The variance of velocity is smaller. Small variations in velocity are observed over the curve during the rainfall as evident from the figure. These results provide different insights into the development, understanding, and evolution of the velocity shockwaves, which are vital for traffic planning and management. Thus, the methodology of this study can be used to analyze highway efficiency.

5. Discussion

In this study, we shed light on the practical utility of the continuum macroscopic model (NHSRM). The usefulness and effectiveness of the NHSRM are demonstrated to understand evolving traffic dynamics related to the geometry of a highway and weather conditions. The methodology of this study helps in gaining valuable insights into how traffic behaves under weather conditions on a highway with a sharp curve.

Certain aspects such as the spatiotemporal evolution of velocity and density, variance of velocity, and travel time of traffic are evaluated in this study subject to assorted weather conditions. Four different weather conditions are considered while two different geometric characteristics characterized by the radius of curvature are evaluated. With geometric road curve of 120 m radius, it is evident in the findings that weather conditions significantly influence the evolution patterns of traffic and congestion levels. It has been observed that dry pavement conditions have a relatively minimal impact on the evolution of traffic flow, the average traffic velocity is settled for a relatively higher value. However, during heavy rainfall, the situation worsens drastically, with traffic experiencing considerable disruptions and congestion due to reduced road grip and visibility challenges.

Further, the impact of adverse weather and the R of the curve on the density propagation is assessed. It is observed that the density evolution on dry pavement is smoother and the jam formation is smaller. On the

other hand, when there is an increase in the intensity of rainfall, the jam formation and dissipation times are longer. The impact on upstream traffic is comprehensively analyzed and discussed. It is observed that upstream traffic is subject to prolonged jams and velocity drops as the rainfall intensity increases.

In addition, the relationship between weather intensity and travel time is explored. Unsurprisingly, the results indicate that travel time elevates with the increase in the intensity of rainfall. The insights of this study are particularly significant for policymakers and traffic planners as accurate travel time predictions are performed, allowing for better planning of routes and improved efficiency on highways.

Furthermore, a significant finding of the study relates to variations in velocity during different weather conditions. Notably, the results reveal that heavy rainfall causes considerable fluctuations in velocity compared to dry weather conditions. With this analysis, the impact of curves during rainfall on upstream traffic is better evaluated. It is noted that after 600 s into the analysis when the impacts of weather conditions are introduced, variations in velocity are maximum upstream later in the time.

In the second scenario with curve $R = 500$ m, the traffic dynamics are different from the previous scenario. With an increase in the R of the curve, the impact of rainfall on velocity drops, jam formation, and travel time is significantly reduced. In this scenario, it is noted that velocity breakdowns are minimal when the intensity of rainfall increases. There are velocity breakdowns, but they are significantly smaller than that with curve $R = 120$ m. However, the velocity evolution is quicker resulting in smoother flow operations.

The density evolution improves with the increase in the radius of the curve. With curve $R = 500$ m, the density evolution is quicker, and the jam propagation upstream from the curve is significantly reduced. This is obvious as the tighter curves allow less flow while the wider curves have a low impact on the flow. Moreover, with the increase in the intensity of rainfall, the formation time of the jam upstream of the curve is somehow impacted. These results provide significant understanding and insights into traffic dynamics in various weather conditions. In general, the traffic dynamics of highway with curve $R = 500$ m are smoother compared to that with curve $R = 120$ m.

The travel time of the highway is assessed with curve $R = 500$ m. It has been observed that the travel time and other characteristics are impacted by the rainfall intensity, however, compared to curve $R = 120$ m, the travel time is enhanced, which is due to the wider curve.

The results of this study are vital and benefit weather adaptive control applications to manage traffic effectively. Having weather conditions incorporated in the model, the predictions of traffic patterns allow to perform better traffic management in real-time, dynamic management can be performed by adjusting traffic signals, implementing lane management strategies based on prevailing traffic conditions, and regulating speed limits. In all, this study advances the understanding of traffic dynamics in various weather conditions and quantifies their impacts on the velocity and density evolution and travel time of traffic.

Continuum models play a crucial role in efficiently planning and managing traffic. This study highlights a practical application, demonstrating the versatility of these models for various uses. Specifically, they can be adapted to account for mixed traffic scenarios involving both Human-Driven Vehicles (HDVs) and Connected and Autonomous Vehicles (CAVs). The introduction of CAVs significantly alters conventional dynamics, impacting the Level of Service (LOS). Consequently, there is a need for methodologies to assess LOS in the presence of CAVs using continuum models. Additionally, new control strategies, such as regulating traffic based on the headway distance of CAVs, can be proposed. However, it is essential to modify continuum models to incorporate these strategies effectively.

6. Conclusion

In this paper, a macroscopic continuum traffic flow model was employed to investigate the impacts of weather conditions on traffic flow on a highway with a sharp curve of 120 m radius, and wider curve with 500 m radius. For dry, light rainfall, moderate rainfall, and heavy rainfall weather conditions, the NHRSM is analyzed. With 120 m, the impact of the curve on upstream traffic in dry weather is minimal. While during light rainfall smaller impact than the dry weather is observed. The situation during moderate rainfall drastically worsens, sharp velocity breakdowns and a decline in the average velocity was noted. Whereas, as expected during heavy rainfall the dynamics drastically change, and the traffic upstream and well as on downstream were deteriorating. However, this situation was enhanced with 500 m radius, the density and velocity evolution is quicker, and less traffic is impacted in the upstream. The resulted as the road geometric curve is wider. The variations in traffic are smaller as compared with 120 m.

The traffic travel time was analyzed for four different weather conditions. It is noteworthy that as the rainfall intensity increases, a drastic increase in travel time occurs. The travel time of the geometric curve, 120 m, varies from as low as 15 s to 200 s. While with a curve of 500 m radius, the travel time for all weather conditions is between 20 s to 60 s. It has been noted that not only the variance of velocity increased with the intensity of rainfall, but the variance of velocity in upstream traffic drastically increased with 120 m radius. This confirms that any change in traffic downstream significantly impacts traffic flow upstream during different weather conditions. This is important to understand and analyze for effective traffic planning and management. Further, it is important to be utilized in automated vehicles for traffic flow amelioration and cruise control for effective traffic dissemination.

CRediT authorship contribution statement

Waheed Imran: Formal analysis, Data curation, Conceptualization, Funding acquisition, Investigation, Methodology, Project administration, Resources, Software, Supervision, Validation, Visualization, Writing – original draft, Writing – review & editing. **Zawar H. Khan:** Formal analysis, Methodology, Project administration, Supervision, Writing – review & editing. **Daud Khan:** Conceptualization, Investigation, Methodology, Writing – original draft. **Usman Ghani:** Formal analysis, Investigation, Writing – original draft. **Tahseen Bashir:** Investigation, Software, Validation.

Declaration of competing interest

The authors declare that they have no known competing financial interests or personal relationships that could have appeared to influence the work reported in this paper.

Data availability

Data will be made available on request.

References

AASHTO, 2011. Policy on Geometric Design of Highways and Streets. e American Association of State Highway and Transportation Officials. AASHTO Green Book, Washington DC, USA.

Afrin, Tanzina, Yodo, Nita, 2020. A survey of road traffic congestion measures towards a sustainable and resilient transportation system. Sustainability 12 (11), 4660.

Al-nasur, Sadeq J., Wadoo, Sabiha Amin, Shende, Apoorva, 2008. Pedestrian Dynamics: Feedback Control of Crowd Evacuation. Understanding Complex Systems. Springer.

Aw, AA.T.M., Rascle, Michel, 2000. Resurrection of" second order" models of traffic flow. SIAM J. Appl. Math. 60 (3), 916–938.

Basak, Kakali, Hetu, Seth N, Azevedo, Carlos Lima, Loganathan, Harish, Toledo, Tomer, Ben-Akiva, Moshe, et al., 2013. Modeling reaction time within a traffic simulation model. In: 16th International IEEE Conference on Intelligent Transportation Systems. ITSC 2013, IEEE, pp. 302–309.

Brackstone, Mark, McDonald, Mike, 2007. Driver headway: How close is too close on a motorway? Ergonomics 50 (8), 1183–1195.
Brilon, Werner, Ponzlet, Martin, 1996. Variability of speed-flow relationships on German autobahns. Transp. Res. Rec. 1555 (1), 91–98.
Cantarella, Giulio Erberto, de Luca, Stefano, Di Gangi, Massimo, Di Pace, Roberta, Memoli, Silvio, 2014. Macroscopic vs. mesoscopic traffic flow models in signal setting design. In: 17th International IEEE Conference on Intelligent Transportation Systems. ITSC, IEEE, pp. 2221–2226.
Daganzo, Carlos F., 1995. Requiem for second-order fluid approximations of traffic flow. Transp. Res. B 29 (4), 277–286.
Helbing, Dirk, Hennecke, Ansgar, Shvetsov, Vladimir, Treiber, Martin, 2001. MASTER: Macroscopic traffic simulation based on a gas-kinetic, non-local traffic model. Transp. Res. B 35 (2), 183–211.
Henein, Colin Marc, White, Tony, 2010. Microscopic information processing and communication in crowd dynamics. Phys. A 389 (21), 4636–4653.
Hoogendoorn, Serge P., Bovy, Piet H.L., 2001. State-of-the-art of vehicular traffic flow modelling. Proc. Inst. Mech. Eng. Part I: J. Syst. Control Eng. 215 (4), 283–303.
Hou, Tian, Mahmassani, Hani S, Alfelor, Roemer M, Kim, Jiwon, Saberi, Meead, 2013. Calibration of traffic flow models under adverse weather and application in mesoscopic network simulation. Transp. Res. Rec. 2391 (1), 92–104.
Hranac, Robert, Sterzin, Emily, Krechmer, Daniel, Rakha, Hesham A, Farzaneh, Mohamadreza, et al., 2006. Empirical Studies on Traffic Flow in Inclement Weather. United States. Federal Highway Administration.
Ibrahim, Amal T., Hall, Fred L., 1994. Effect of adverse weather conditions on speed-flow-occupancy relationships, no. 1457.
Imran, Waheed, Khan, Zawar H, Gulliver, T Aaron, Alam, Muhammad, Khattak, Khurram S, 2023. Non-homogeneous traffic characterization based on driver reaction and stimuli. Transp. Res. Interdisc. Perspect. 21, 100858.
Imran, Waheed, Khan, Zawar H, Gulliver, T Aaron, Khattak, Khurram S, Nasir, Hassan, 2020. A macroscopic traffic model for heterogeneous flow. Chinese J. Phys. 63, 419–435.
Imran, Waheed, Tettamanti, Tamás, Varga, Balázs, Bifulco, Gennaro Nicola, Pariota, Luigi, 2024. Macroscopic modeling of connected, autonomous and human-driven vehicles: A pragmatic perspective. Transp. Res. Interdisc. Perspect. 24, 101058. http://dx.doi.org/10.1016/j.trip.2024.101058, URL https://www.sciencedirect.com/science/article/pii/S2590198224000447.
Jiang, Rui, Wu, Qing-Song, 2004. Extended speed gradient model for mixed traffic. Transp. Res. Rec. 1883 (1), 78–84.
Jiang, Rui, Wu, Qing-Song, Zhu, Zuo-Jin, 2002. A new continuum model for traffic flow and numerical tests. Transp. Res. B 36 (5), 405–419.
Kessels, Femke, Kessels, Rauscher, Rauscher, 2019. Traffic Flow Modelling. Springer.
Khan, Zawar H., Gulliver, T. Aaron, 2018. A macroscopic traffic model for traffic flow harmonization. Eur. Transp. Res. Rev. 10 (2), 1–12.
Khan, Zawar H., Gulliver, T. Aaron, 2019. A macroscopic traffic model based on anticipation. Arab. J. Sci. Eng. 44, 5151–5163.
Khan, Zawar Hussain, Gulliver, Thomas Aaron, Imran, Waheed, Khattak, Khurram Shehzad, Altamimi, Ahmed B, Qazi, Azhar, 2022a. A macroscopic traffic model based on relaxation time. Alex. Eng. J. 61 (1), 585–596.
Khan, Zawar H., Imran, Waheed, Azeem, Sajid, S. Khattak, Khurram, Gulliver, T Aaron, Aslam, Muhammad Sagheer, 2019. A macroscopic traffic model based on driver reaction and traffic stimuli. Appl. Sci. 9 (14), 2848.
Khan, Zawar H, Imran, Waheed, Gulliver, Thomas Aaron, Khattak, Khurram S, Wadud, Zahid, Khan, Akhtar Nawaz, 2020. An anisotropic traffic model based on driver interaction. IEEE Access 8, 66799–66812.
Khan, Daud, Khan, Zawar Hussain, Imran, Waheed, Khattak, Khurram Shehzad, Gulliver, Thomas Aaron, 2022b. Macroscopic flow characterization at T-junctions. Transp. Res. Interdisc. Perspect. 14, 100591.
Khan, Zawar H., Shah, Syed Abid Ali, Gulliver, T. Aaron, 2018. A macroscopic traffic model based on weather conditions. Chin. Phys. B 27 (7), 070202.
Ko, Hung-Tang, Liu, Xiao-He, Guo, Ming-Min, Wu, Zheng, 2015. A new traffic model with a lane-changing viscosity term. Chin. Phys. B 24 (9), 098901.
Kordani, A Abdi, Rahmani, Omid, Nasiri, AS Abdollahzadeh, Boroomandrad, Sid Mohammad, 2018. Effect of adverse weather conditions on vehicle braking distance of highways. Civ. Eng. J. 4 (1), 46–57.
Kyte, Michael, Khatib, Zaher, Shannon, Patrick, Kitchener, Fred, 2001. Effect of weather on free-flow speed. Transp. Res. Rec. 1776 (1), 60–68.
Lam, William H.K., Tam, Mei Lam, Cao, Xinqing, Li, Xiangmin, 2013. Modeling the effects of rainfall intensity on traffic speed, flow, and density relationships for urban roads. J. Transp. Eng. 139 (7), 758–770.
Lamm, Ruediger, Choueiri, Elias M., Mailaender, Theodor, 1990. Comparison of operating speeds on dry and wet pavements of two-lane rural highways. Transp. Res. Rec. 1280 (8), 199–207.
Liang, Wei Lien, Kyte, Michael, Kitchener, Fred, Shannon, Patrick, 1998. Effect of environmental factors on driver speed: A case study. Transp. Res. Rec. 1635 (1), 155–161.
Lighthill, Michael James, Whitham, Gerald Beresford, 1955. On kinematic waves II. A theory of traffic flow on long crowded roads. Proc. R. Soc. London. Ser. A. Math. Phys. Sci. 229 (1178), 317–345.
Liu, Guoqing, Lyrintzis, Anastasios S., Michalopoulos, Panos G., 1998a. Improved high-order model for freeway traffic flow. Transp. Res. Rec. 1644 (1), 37–46.
Liu, Guoqing, Lyrintzis, Anastasios S., Michalopoulos, Panos G., 1998b. Improved high-order model for freeway traffic flow. Transp. Res. Rec. 1644 (1), 37–46.
Maerivoet, Sven, De Moor, Bart, 2005. Transportation planning and traffic flow models. arXiv preprint physics/0507127.
Maze, Thomas H., Agarwal, Manish, Burchett, Garrett, 2006. Whether weather matters to traffic demand, traffic safety, and traffic operations and flow. Transp. Res. Rec. 1948 (1), 170–176.
Moura, Carlos A. de, Kubrusly, Carlos S., 2012. The Courant-Friedrichs-Lewy (CFL) Condition: 80 Years After Its Discovery. Birkhäuser Basel.
Nagel, Kai, Wagner, Peter, Woesler, Richard, 2003. Still flowing: Approaches to traffic flow and traffic jam modeling. Oper. Res. 51 (5), 681–710.
Ngoduy, Dong, 2013. Instability of cooperative adaptive cruise control traffic flow: A macroscopic approach. Commun. Nonlinear Sci. Numer. Simul. 18 (10), 2838–2851.
Papageorgiou, Markos, Blosseville, Jean-Marc, Hadj-Salem, Habib, 1989. Macroscopic modelling of traffic flow on the Boulevard Périphérique in Paris. Transp. Res. B 23 (1), 29–47. http://dx.doi.org/10.1016/0191-2615(89)90021-0.
Payne, H.J., 1971. Models of Freeway Traffic and Control. Mathematical Models of Public Systems. Simulation Councils. Inc Vista, CA, USA.
Ping, Y.I., John, L.U., Zhang, Yucheng, Huapu, L.U., 2004. Safety-based capacity analysis for Chinese highways: A preliminary study. IATSS Res. 28 (1), 47–55.
Qingtao, Zhai, Hongxia, Ge, Rongjun, Cheng, 2018. An extended continuum model considering optimal velocity change with memory and numerical tests. Phys. A 490, 774–785.
Qu, Dayi, Chen, Xiufeng, Yang, Wansan, Bian, Xiaohua, et al., 2014. Modeling of car-following required safe distance based on molecular dynamics. Math. Probl. Eng. 2014.
Richards, Paul I., 1956. Shock waves on the highway. Opera. Res. 4 (1), 42–51.
Richtmyer, Robert D., 1957. Difference Methods for Initial-Value Problems, vol. 4, Interscience Publishers.
Shahdah, Usama, Fu, Liping, 2010. Quantifying the mobility benefits of winter road maintenance–a simulation based analysis. In: TRB 89th Annual Meeting Compendium of Papers DVD.
Song, Jiah, Karni, Smadar, 2019. A second order traffic flow model with lane changing. J. Sci. Comput. 81 (3), 1429–1445.
Tang, Tie-qiao, Li, Chuan-yao, Huang, Hai-jun, Shang, Hua-yan, 2011. Macro modeling and analysis of traffic flow with road width. J. Central South Univ. 18 (5), 1757–1764.
Toro, Eleuterio Francisco, et al., 1996. On Glimm-Related Schemes for Conservation Laws. Technical Report.
Trans. Research Board, 2010, Transportation Research Board, National Research Council, Washington, DC, 1207, 000.
Whitham, Gerald Beresford, 2011. Linear and Nonlinear Waves. John Wiley & Sons.
Younes, Maram Bani, 2023. Safe and efficient advising traffic system around critical road scenarios. Int. J. Intell. Transp. Syst. Res. 21 (1), 229–239.
Zhai, Cong, Wu, Weitiao, 2021. A continuous traffic flow model considering predictive headway variation and preceding vehicle's taillight effect. Physica A 584, 126364.
Zhai, Cong, Wu, Weitiao, 2022. A continuum model considering the uncertain velocity of preceding vehicles on gradient highways. Phys. A 588, 126561.
Zhang, H. Michael, 1998. A theory of nonequilibrium traffic flow. Transp. Res. B 32 (7), 485–498.